



A promoting effect of dilution of Pd sites due to gold surface segregation under reaction conditions on supported Pd–Au catalysts for the selective hydrogenation of 1,5-cyclooctadiene



Patricia Concepción ^{a,*}, Saray García ^a, Juan Carlos Hernández-Garrido ^b,
Jose Juan Calvino ^b, Avelino Corma ^{a,c,**}

^a Instituto de Tecnología Química CSIC-UPV, Universidad Politécnica de Valencia, 46022 Valencia, Spain

^b Departamento de Ciencia de los Materiales, Ingeniería Metalúrgica y Química Inorgánica, Universidad de Cádiz, Facultad de Ciencias, Campus Río San Pedro, Puerto Real, 11510 Cádiz, Spain

^c King Fahd University of Petroleum and Minerals, P. O. Box 31261, Dhahran 31261, Saudi Arabia

ARTICLE INFO

Article history:

Received 30 March 2015

Received in revised form 14 July 2015

Accepted 16 July 2015

Available online 11 August 2015

Keywords:

AuPd

CeO₂

Selective hydrogenation

Cyclooctadiene

XPS

Site isolation

ABSTRACT

Restructuration of AuPd/CeO₂ catalysts is observed during 1,5-cyclooctadiene hydrogenation, with gold surface segregation in which gold acts as a diluent of Pd surface sites. The composition of the catalyst influences the catalytic behavior, and an optimum is observed at a Pd/Au molar ratio of 0.13, as determined by X-EDS STEM. Pd–Au/CeO₂ shows higher hydrogenation rates (11.2×10^{-5} mol/g s) versus the unpromoted Pd/CeO₂ catalysts (1.7×10^{-5} mol/g s), and the Pd/TiO₂ (7.5×10^{-5} mol/g s) catalysts used as conventional hydrogenation catalysts. Since the active sites are generated under reaction conditions, characterization of the catalysts after quenching the reaction at specific reaction times was required.

© 2015 Elsevier B.V. All rights reserved.

1. Introduction

A rational way to design solid catalysts will go through the fundamental understanding of the generation of the catalytic active sites and their interaction with reactant and products under reaction conditions. For achieving that, catalysts are many times characterized before being subjected to the reaction and the obtained results are correlated with catalytic activity and selectivity. Following that methodology it is sometimes difficult to establish good structure–reactivity correlations since, as has been reported, structural and chemical modifications of the catalysts can occur under reaction conditions [1–4]. Moreover these changes could in certain cases affect only the catalyst surface [5]. Therefore, knowledge of the catalyst under reaction conditions (operando spectroscopy) or at least as close as possible to reaction conditions, becomes very important. From the point of view of catalyst

characterization techniques, X-ray photoelectron spectroscopy (XPS) is a very powerful spectroscopic tool which gives chemical information from the 6–9 nm outermost surface layers, while infrared spectroscopy (FTIR) of adsorbed molecule, gives specific information about the interaction of molecules with active sites located at the external catalyst surface. Thus, the combination of both spectroscopies will be helpful for better understanding the catalytic behavior at the surface of solids.

In the case of catalysts based on metal nanoparticles, several parameters like particle size and morphology, metal–support interactions, chemical composition i.e. oxidation states, presence of promoters, etc. are of paramount importance for catalysis [6–9]. Moreover, the addition of a second metal to produce bimetallic nanoparticles, has opened more possibilities for engineering catalysts with enhanced activity and selectivity. Important technological areas, including catalytic reforming [10], pollution control, alcohol oxidation [11–13], selective hydrogenation [8,14–16], electro-catalysis in fuel cells [17], among other, are based on bimetallic systems. It has been reported that the synthesis method can direct the formation of bimetallic materials with different final structures like core–shell or alloy formation with markedly different catalytic behavior [1,18]. In the case of bimetallic materials, and even more so when the size of the materials are in the range

* Corresponding author.

** Corresponding author at: Instituto de Tecnología Química CSIC-UPV, Universidad Politécnica de Valencia, 46022 Valencia, Spain.

E-mail addresses: pconcep@upnet.upv.es (P. Concepción), [\(A. Corma\).](mailto:acorma@itq.upv.es)

of the nanometer scale, structural and compositional changes can produce large differences in the catalytic behavior of the nanoparticles. If this is so, one should take into account that metal surface composition and size and shape of those bimetallic catalysts can change during the reaction, being the final catalyst different from the starting one.

In the present study we will show that modifications in the structure of monometallic Pd and Au and bimetallic AuPd catalysts occur during the hydrogenation of 1,5-cyclooctadiene, with an impact on the catalytic activity. This has been found by stopping the reaction during the catalytic process and following the possible change by XPS, HRTEM and FTIR spectroscopic characterization.

The selective hydrogenation of dialkenes and/or alkynes to monoalkenes, continues to attract attention due to practical importance and fundamental interest [16,19,20]. While Pd exhibits the highest activity toward alkenes in dialkenes or alkynes hydrogénations, the selectivity toward monoalkenes with Pd significantly decreases when working at high conversions of dialkenes or alkynes [20]. Thus, considerable attention has been paid to factors which can improve the selectivity of Pd catalysts for the above hydrogenation reactions. The reaction selectivity during dialkenes hydrogenation to alkenes is determined by the rates of alkene desorption and hydrogenation. Taking into account that the interaction of adsorbed molecules depends on the morphology of the surface i.e. the coordination number of the surface atoms, which depends among others, on the metal particle size, addition of other metals, etc., metal particle size effects [21,22] as well as the addition of other metals to Pd [16,23,24] have been studied as one way to improve its catalytic performance. Among bimetallic Pd catalysts, the Pd–Au system has been extensively investigated for selective hydrogenations [16,19,20,23–26] as well as for oxidation reactions [11,18,27,28]. The enhanced catalytic behavior observed in the bimetallic AuPd system has usually been explained due to formation of a core/shell structure [29,30], alloy formation [24,31,32], selective poisoning of the Pd surface [16,33,34] and changes in metal dispersion and morphology of the particle [26]. On the other hand, the impact of metal–support interactions on the catalytic behavior of supported metal particles is well known for several processes. In this sense, ceria has been reported as a very active support for oxidation as well as for hydrogenation reactions [35–37]. Interestingly, very few studies [38] have been reported for the hydrogenation of cyclodienes or dialkenes using ceria supported catalysts, therefore our interest has been driven on this reaction, as a test reaction for studying monometallic and bimetallic Au–Pd/CeO₂ catalysts.

2. Experimental

2.1. Catalyst preparation

TiO₂ was a commercial sample (Degussa P25, mainly anatase). Nanocrystalline CeO₂ was prepared by thermolysis of an acidified Ce(NO₃)₄ solution followed by redispersion, according to Ref. [36]. The dispersion was purified and concentrated using an ultrafiltration cell equipped with a 3KD membrane. The purification was monitored by the residual acidity of the dispersion, determined by an acid titration of the supernatant after ultra-centrifugation at 50 000 rpm for 6 h. 0.36 wt% Au was deposited on the nanoparticulated cerium oxide by the following procedure: Nanocrystalline CeO₂ powders (2 g) were added into an HAuCl₄ aqueous solution (Aldrich, 99.9%) whose pH was fixed at 7.7 by addition of a 0.2 M NaOH solution. The mixture was stirred for 12 h, statically aged for 6 h and then washed with deionized water, filtered and dried at 120 °C in air for 12 h. Samples of 0.1 and 0.24 wt% Pd supported

on CeO₂ and 0.13 and 0.23 wt% Pd supported on TiO₂ were prepared by a deposition–precipitation method by mixing CeO₂ or TiO₂ powders with appropriate amounts of aqueous solutions of Pd(NO₃)₂·xH₂O (Aldrich, 99.9%) at a fixed pH (7.6±0.3) adjusted with 0.35 wt% NH₄OH solution. The mixtures were stirred for 12 h and statically aged for 6 h. Then they were washed with deionized water, filtered and dried at 120 °C in air for 12 h.

A series of Pd–Au/CeO₂ catalysts with of 0.2, 0.17, 0.10 and 0.05 wt% of Pd loading and 0.36 wt% Au were prepared by the deposition–precipitation method of Au/CeO₂ with Pd(NO₃)₂. Typically, the air dried Au/CeO₂ sample was added to an aqueous solutions of Pd(NO₃)₂ at a fixed pH (7.6±0.3), adjusted with 0.35 wt% NH₄OH. The mixture was stirred for 12 h and statically aged for 6 h. The samples were then washed, filtered, and dried at 120 °C for 12 h. The above samples dried in air at 120 °C for 12 h, are referred to as prepared samples and labeled as X% Pd–Y% AuCe, where X, Y represent the weight percent of each element as determined by ICP. The H₂ pre-reduced sample was obtained by further treatment of the air dried sample in flowing H₂ at 200 °C for 2 h. Once reduced, the samples were kept under N₂ atmosphere until further use in catalytic tests or spectroscopic characterization techniques. On the other hand, the as prepared Pd–Au/CeO₂ samples were studied immediately after preparation.

2.2. Catalyst characterization

Gold and palladium loadings were determined by inductively coupled plasma atomic emission spectroscopy (ICP-AES).

X-ray photoelectron spectra of the catalysts were recorded with a SPECS spectrometer equipped with a Phoibos 150MCD multichannel analyzer, using MgK α (1253.6 eV) irradiation. The spectra were recorded with an X-ray power of 50 mW in order to avoid fotoreduction of the gold species. The residual pressure in the analytical chamber was maintained below 10⁻⁹ mbar during data acquisition. The binding energies of Au 4f and Pd 3d were corrected for surface charging by referencing them to the energy of Ce3d_{5/2} v1 peak of the ceria support set at 882.178 eV in case of CeO₂ supported samples and to the Ti2p_{3/2} XPS peak set at 458.5 eV in case of TiO₂ supported samples. Peak intensities have been calculated after nonlinear Shirley-type background subtraction and corrected by the transmission function of the spectrometer. CasaXPS software has been used for spectra deconvolution.

FTIR spectra have been collected with a FTS-40A BioRad spectrometer equipped with a DTGS detector (4 cm⁻¹ resolution, 32 scans). An IR cell allowing *in situ* treatments under controlled atmospheres and temperatures from -176 °C to 500 °C has been connected to a vacuum system with gas dosing facility. Self-supporting pellets (ca. 10 mg cm⁻²) were prepared from the sample powders and treated at 50 °C under dynamic vacuum (10⁻⁴ mbar). After activation, the samples were cooled down to -176 °C followed by CO dosing at increasing pressures (0.4–8.5 mbar) and the IR spectrum recorded after each dosage.

Electron microscopy studies (HRTEM, HAADF-STEM, XEDS-STEM) were performed in a JEOL2010F microscope. The structural resolution in HRTEM mode of this microscope is 0.19 nm. The crystallographic information in HRTEM images was analyzed from Digital Diffraction Patterns calculated from selected regions. Local, subnanometer scale, chemical analysis of the catalysts was done by recording X-EDS spectra using an electron probe with a 0.5 nm diameter.

XPS, electron microscopy and FTIR studies have also been done on samples after catalytic performance. For that purpose, the reaction has been stopped at specified times, the reactant mixture removed and analyzed by GC and the catalysts recovered by filtration followed by drying in vacuum and keeping in a N₂ atmosphere until use in characterization studies.

2.3. Selective hydrogenation of 1,5-cyclooctadiene

The liquid phase hydrogenation of 1,5-cyclooctadiene (COD) was carried out in a reinforced glass batch reactor (2.5 mL, SUPELCO) closed with a Teflon septum and equipped with a pressure gauge and a side arm with an on-off lock. A micro-syringe can be allowed to inject and withdraw liquid or gas through the lock. Typically, the reactor with 7 mg (80–120 mesh) of the catalyst and 56.1 mg (0.5 mmol) 1,5-cyclooctadiene in n-octane (1.0 mL) was purged with hydrogen for 3 times and then hydrogen was introduced up to 10 bar. The reaction was assumed to start when the reactor was introduced into the oil bath at 50 °C and vigorously stirred (ca. 1000 rpm). At a desired reaction time, 20 μL samples were taken through the micro-syringe and analyzed with a HP gas chromatograph equipped with a FID and a Carbowax 20M capillary column. The mole calibration factors of n-cyclooctane ($f_{COA} = 1.00$), cyclooctene ($f_{COE} = 0.98$), 1,3-cyclooctadiene ($f_{1,3COD} = 0.77$) and 1,5-cyclooctadiene ($f_{COD} = 0.77$) were determined by standard solution of these components. Isomerization of 1,5-cyclooctadiene to 1,3-cyclooctadiene is observed as a primary product on all catalysts.

3. Results and discussion

3.1. Pd/CeO₂ catalysts

The as prepared Pd/CeO₂ samples show no catalytic activity for the hydrogenation of COD, in opposite to Pd/TiO₂ samples which give conversions close to 100% at the same Pd loading (Fig. 1A). XPS characterization of the samples prior to catalytic test (Table 1) shows in both cases the presence of Pd²⁺ (BE 337–336 eV) [39,40] making then difficult to explain their different catalytic behavior from the analysis of the fresh catalysts. However, when the samples were analyzed by XPS after stopping the reaction at specific reaction times, clear differences can be observed between the two samples. Pd⁰ (BE 334.5 eV) [39,40] is detected in the PdTiO₂ sample stopping the reaction at 50 min, while only Pd²⁺ was found in the PdCeO₂ sample even after 160 min reaction time. These results would be consistent with the high potential of CeO₂ to stabilize cationic species and could help to explain the catalytic behavior displayed in Fig. 1A by assuming Pd⁰ sites, generated under reaction conditions, as the catalytic active sites for the hydrogenation of COD.

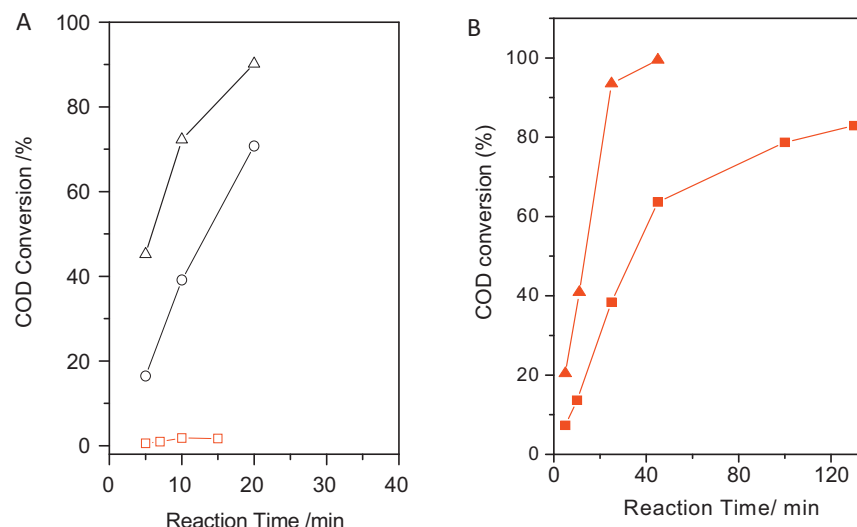


Fig. 1. (A) COD conversion versus reaction time on 0.1PdCe (□), 0.13PdTi (○) and 0.24PdTi (△) samples. (B) COD conversion versus reaction time on ex situ reduced samples: 0.1PdCe-H₂ (■) and 0.24 PdCe-H₂ (▲) samples.

Since the lack of activity observed with PdCeO₂ samples could be related, in a first approximation, to the absence of reduced Pd species, one could then increase the amount of reduced Pd species, and therefore their catalytic activity, by reducing the samples in H₂. Ex situ reduction at 200 °C in H₂ leads to the formation of Pd⁰ in PdCeO₂, as confirmed by XPS analysis (Table 1) and, consequently to an increase in the hydrogenation activity (Fig. 1B). However when compared with Pd/TiO₂, at the same Pd loading (0.1 wt%), the reaction rate of the reduced 0.1PdCe-H₂ sample (1.7×10^{-5} mol/g s) is still lower than the value observed with the 0.13PdTi sample (4.4×10^{-5} mol/g s) or 0.13PdTi-H₂ sample (7.5×10^{-5} mol/g s). Thus, the different catalytic activity of Pd/CeO₂ and Pd/TiO₂ samples cannot be simply explained by a difference in the amount of Pd⁰ species under reaction conditions (see Table 1), but other factors like metal morphology, size and shape, may also play a role, being those under investigation. The selectivity to products differs slightly in the 0.13PdTi versus 0.1PdCe sample (Fig. S1, supplementary information). In particular, the selectivity to isomerization product (1,3-cyclooctadiene) is lower in the PdTi sample while their selectivity to cyclooctane is higher. In accordance with the above reported differences in activity, the differences in selectivity agree with the postulated morphological factors.

As the activity and selectivity of Pd can be modified by introduction of promoters, we have explored this possibility here by synthetizing bimetallic Pd–Au materials.

3.2. Pd–Au/CeO₂ catalysts

An air dried Au/CeO₂ (0.36 wt% Au) sample was impregnated with different Pd loadings (0.05–2 wt%) within a molar ratio Pd:Au of 0.25–1. XPS data of the as prepared samples (Table 2) show the presence of Au⁰ (84–83.6 eV) and Au⁺ (85.6 eV) [36,41] in both Au/CeO₂ and Pd–Au/CeO₂ samples. Meanwhile Pd²⁺ and Pd⁰ are both present in the as prepared Pd–Au/CeO₂ samples, while only Pd²⁺ was detected in Pd/CeO₂ (see Table 1). Thus, the presence of Au seems to favor the reduction of Pd²⁺ to Pd⁰ even during sample impregnation/drying. On the other hand, the Pd/Au molar ratio determined by XPS increases (except in the 0.2Pd–0.36AuCe sample) when increasing the Pd loading, as expected according to the preparation method in which Pd is added on the previously prepared Au/CeO₂ sample.

Ex situ reduction of the bimetallic samples in H₂ at 200 °C increased the amount of Pd⁰ species, and reduced all Au species

Table 1

XPS data of as prepared and ex situ reduced Pd/CeO₂ and Pd/TiO₂ samples, before and after stopping the reaction at specific reaction times.^e

Sample	Pd (wt%) ^a	Pd/(Me + O) ^b	Before catalytic test			After catalytic test			t (min)	%C ^e
			Pd/(Me + O) ^c	Pd ²⁺ (%) ^d	Pd ⁰ (%) ^d	Pd/(Me + O) ^c	Pd ²⁺ (%) ^d	Pd ⁰ (%) ^d		
0.1PdCe	0.096	0.0005	0.001	337.2 (100)	–	n.d.	n.d.	–	n.d.	1.03
0.24PdCe	0.24	0.0013	0.0026	337.2 (100)	–	0.0076	337.8 (100)	–	160	65
0.13PdT	0.13	0.0003	0.0005	336.0 (100)	–	n.d.	n.d.	–	n.d.	44.83
0.23PdT	0.23	0.0005	0.0013	336.0 (100)	–	0.0013	336.5 (61.7)	334.5 (38.3)	50	97.0
0.1PdCe-H ₂	0.096	0.0005	0.001	337.5 (61.4)	334.9 (38.5)	0.0015	337.0 (59.4)	334.7 (40.6)	130	65
0.24PdCe-H ₂	0.24	0.0013	0.0026	n.d.	0.0048	337.0 (38.1)	334.3 (61.9)	–	11	44.83
0.13PdT-H ₂	0.13	0.0003	0.0005	337.0 (61.4)	333.6 (38.6)	0.0008	336.6 (61.2)	334.2 (38.8)	10	35.24

^a Pd weight percent determined by ICP.

^b Surface composition (atomic ratio) determined by ICP; Me = Ti or Ce.

^c Surface composition (atomic ratio) determined by XPS; Me = Ti or Ce.

^d BE (eV) of each oxidation state. Values in brackets represent the atomic percent of each oxidation state determined by XPS.

^e Conversion of COD (%C) at reaction time (t) at which the sample has been characterized.

Table 2

XPS data of as prepared and ex situ reduced Pd–Au/CeO₂ samples before catalytic test.

Sample	Pd/Au ^a	Pd/Au ^b	Pd 3d5/2 ^c		Au4f7/2 ^c		
			Pd ²⁺ (%)	Pd ⁰ (%)	Au ⁰ (%)	Au ⁺ (%)	Au ³⁺ (%)
0.00Pd–0.36AuCe	0	0	–	–	84.1 (76.1)	85.6 (23.8)	–
0.05Pd–0.36AuCe	0.25	1.28	337.4 (100)	–	83.8 (83.0)	85.2 (17.0)	–
0.10Pd–0.36AuCe	0.5	3.5	337.3 (85.7)	334.7 (14.3)	83.6 (67.6)	85.8 (32.4)	–
0.17Pd–0.36AuCe	0.87	7.77	337.3 (88.2)	335.3 (11.8)	83.6 (67.6)	85.8 (32.4)	–
0.20Pd–0.36AuCe	1	5.8	n.d.	–	n.d.	–	–
0.05Pd–0.36AuCe-H ₂	0.25	4	336.5 (64.5)	334.0 (35.5)	83.1 (100)	–	–
0.10Pd–0.36AuCe-H ₂	0.5	7.4	337.0 (53.3)	335.2 (46.7)	83.3 (100)	–	–
0.17Pd–0.36AuCe-H ₂	0.87	3.16	337.2 (47.7)	335.2 (52.3)	83.2 (100)	–	–
0.20Pd–0.36AuCe-H ₂	1	8.1	337.0 (74.2)	334.8 (25.8)	83.5 (100)	–	–

^a Surface composition (atomic ratio) determined by ICP.

^b Surface composition (atomic ratio) determined by XPS.

^c BE (eV) of each oxidation state. Values in brackets represent the atomic percent of each oxidation state determined by XPS.

to Au⁰ (**Table 2**). A change in the Pd/Au metal surface composition is also observed by XPS, pointing to a re-dispersion of both metals during H₂ reduction. However no clear trend is observed in the surface distribution of both metals (Pd/Au ratio) during reduction conditions, with the metal loading. In the XPS core level binding energy (BE) the 84.1 eV of metallic gold, observed in the Pd free Au/CeO₂ sample, shifts to lower BE in the presence of Pd, 83.6 ± 0.2 eV in the as prepared samples and to 83.2 ± 0.2 eV in the reduced ones. This shift could be related to particle size effects or to an electronic interaction between Pd and Au. In the case of palladium, Pd⁰ BE between 334.5 and 335.5 eV are observed in the as prepared as well as in reduced samples, however the different Pd BE are not clearly associated to the presence of gold or to the reduction treatment. Thus, according to the XPS results no clear evidence about the presence of any Au–Pd particle interaction or alloy formation can be deduced.

The catalytic activity of the Au/CeO₂ catalyst for the hydrogenation of COD is very low, even after H₂ reduction at 200 °C (8% conversion at 160 min). As prepared Pd–Au/CeO₂ samples shows also low activity. However activity increases drastically after ex situ reduction in H₂ (**Fig. 2**), being this activity higher than on reduced Pd/CeO₂ samples and even higher than on the reduced Pd/TiO₂ samples (at the same Pd loading (0.1 wt%)), with initial reaction rates of 11.2 × 10⁻⁵ mol/g s for the 0.1Pd–0.36AuCe-H₂ sample. Moreover the initial reaction rate of reduced Pd–Au/CeO₂ samples follows a volcano type curve when plotted versus the nominal Pd loading (i.e. Pd/Au molar ratio), with a maximum at a Pd/Au molar ratio of 0.5 (**Fig. 3**). The selectivity to isomerization and hydrogenation products changes also with catalyst composition (Fig. S2 in supplementary information). Specifically the selectivity toward isomerization is lower in all Pd–Au/CeO₂ samples versus the un-promoted PdCe sample. Interestingly the

lowest 1,3-cyclooctadiene selectivity is observed on the most active catalysts (i.e. with a Pd/Au molar ratio of 0.5), while the selectivity to cyclooctane is higher on this sample. In order to understand the promoting effect of gold on the catalytic activity observed with AuPd/CeO₂ bimetallic catalysts, and taking into account the results presented in the first part of this work which showed that the catalysts underwent dramatic changes under reaction conditions,

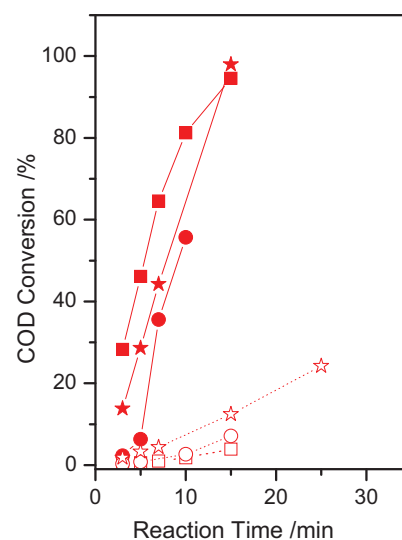


Fig. 2. COD conversion versus reaction time on as prepared (open symbol) and ex situ reduced (full symbols) 0.05Pd–0.36AuCe (○, ●), 0.1Pd–0.36AuCe (□, ■) and 0.17Pd–0.36AuCe (☆, ★) samples.

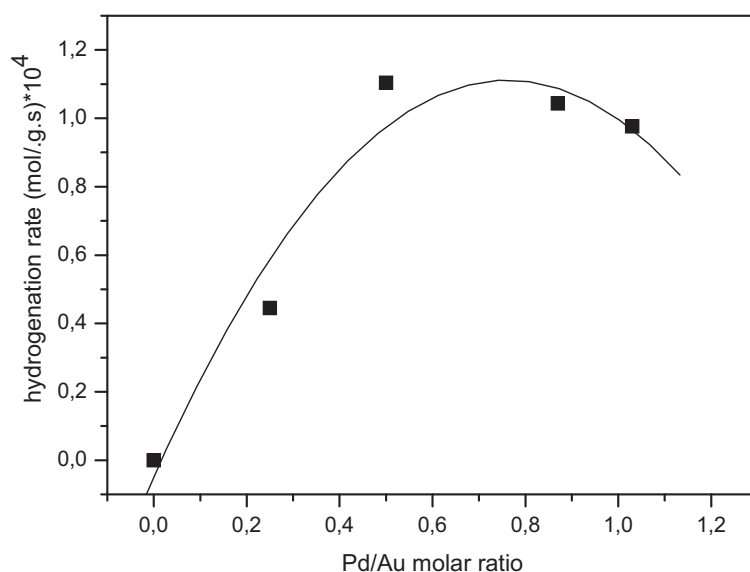


Fig. 3. Variation of the reaction rate in reduced Pd–Au/CeO₂ samples versus the Pd/Au molar ratio determined by ICP.

characterization of the samples has been performed after stopping the reaction at specific reaction times.

From those data, we can conclude that under reaction conditions, and according to XPS results, a modification of the oxidation state of the metal surface sites and a surface restructuration of the AuPd/CeO₂ catalysts is observed (see Table 3 and Figs. S3a, b and S4a, b in supplementary information). The amount of Pd⁰ species increases in both the as prepared and ex situ reduced samples, to around 53% and 70% respectively, due to the in situ reduction of Pd²⁺ ions under reaction conditions. On the other hand, a gold surface segregation has been observed after reaction, being more evident on the reduced samples, giving a Pd/Au molar ratio of ~2.5 in all cases. This agrees with the much lower surface energy of Au versus Pd [42], favoring surface enrichment by Au. However the different catalytic behavior shown in Fig. 2 for the as prepared and ex situ reduced samples, cannot be explained according to the XPS data, as both samples show similar XPS results once exposed to reaction conditions. Therefore further characterization work was required for explaining the reactivity behavior. Since different morphology of the exposed metal particle, such as crystallographic phases, coordination number of the surface atoms, particle size effects, etc. has been reported to influence the catalytic behavior of Pd samples in selective hydrogenation reactions, electron microscopy studies as well as IR studies of CO adsorption as probe molecule have been performed on the as prepared and ex situ reduced 0.1Pd–0.36AuCe sample after stopping the reaction at 15 min. Both techniques are

very suitable for analyzing particle size and morphology and determining surface properties.

Electron microscopy results show the presence of both large and very small Au nanocrystals in the as prepared 0.1Pd–0.36AuCe sample (non-active sample) after stopping the reaction at 15 min reaction time. Data included in Fig. 4 illustrate the case of the large Au nanoparticles. The X-EDS spectrum recorded from this large, very high intensity area confirms that it corresponds to Au. Likewise, the combination of HRTEM and XEDS results recorded on the same areas of the catalyst also suggests the occurrence of very small gold nanocrystals. Thus, Fig. 5 shows a HRTEM image in which a CeO₂ nanoparticle is unambiguously identified from the spots observed in the corresponding DDP (shown as inset). The X-EDS spectrum recorded from the same crystallite, using a 0.5 nm probe in STEM mode, shows Au in addition to Ce and O peaks. Since no gold particle is clearly visible in the analyzed area, we must conclude that gold must be present in that area in a very highly dispersed state. Image simulation data [43] indicate that the detection limit in HRTEM images of metal nanoparticles supported on ceria is roughly below 1 nm. Small patches of material with diameter below 1 nm have been also detected by HRTEM on the border of the CeO₂ nanocrystals which suggest the occurrence of subnanometer-sized Au nanocrystals (Fig. S5, supplementary information). Pd particles could not be observed in the images of the as-prepared catalyst. Likewise, X-EDS from large regions in this catalyst did not show the presence of Pd peaks, this suggesting that probably Pd is in the

Table 3

XPS data of as prepared and ex situ reduced Pd–Au/CeO₂ samples after stopping the reaction at specific reaction times.^a

Sample	<i>t</i> (min)	C (%) ^a	Pd/Au ^b	Pd3d5/2 ^c		Au4f7/2 ^c		
				Pd ²⁺ (%)	Pd ⁰ (%)	Au ⁰ (%)	Au ⁺ (%)	Au ³⁺ (%)
0.05Pd–0.36AuCe	15	7.13	2.4	337.4 (45.1)	334.3 (54.9)	83.9 (77.6)	85.6 (22.4)	–
0.10Pd–0.36AuCe	15	3.91	3	337.2 (47.9)	334.7 (52.1)	83.8 (57.1)	85.6 (42.9)	–
0.17Pd–0.36AuCe	n.d.		n.d.	n.d.	n.d.	n.d.	n.d.	n.d.
0.20Pd–0.36AuCe	n.d.		n.d.	n.d.	n.d.	n.d.	n.d.	n.d.
0.05Pd–0.36AuCe-H ₂	15	54.04	2.2	336.8 (42.1)	334.6 (57.9)	84.0 (68.6)	–	86.0 (31.4)
0.10Pd–0.36AuCe-H ₂	15	94.55	2.57	337.6 (27.8)	335.0 (72.2)	84.2 (67.8)	–	86.5 (32.2)
0.17Pd–0.36AuCe-H ₂	7	39.2	2.23	337.2 (28.5)	334.7 (71.5)	83.3 (55.5)	–	86.1 (44.5)
0.20Pd–0.36AuCe-H ₂	7	55.35	2.4	337.5 (41.7)	334.8 (58.3)	83.8 (77.9)	–	86.1 (22.1)

^a Conversion of COD (C) at reaction time (*t*) at which the sample has been characterized.

^b Surface composition (atomic ratio) determined by XPS.

^c BE (eV) of each oxidation state. Values in brackets represent the atomic percent of each oxidation state determined by XPS.

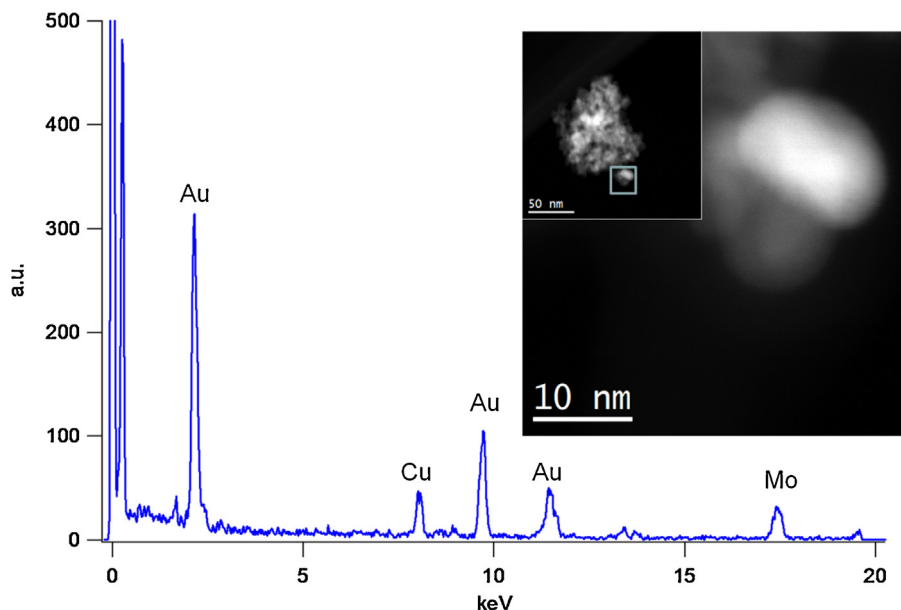


Fig. 4. HAADF-STEM of the as prepared 0.1Pd–0.36AuCe sample after 15 min reaction time. The XEDS-spectrum was recorded on the large crystallite shown as enlargement. Copper and molybdenum signals arise from the specimen holder and the coated Mo-grids used, respectively.

form of larger crystallites, statistically hard to find due to the very low Pd content. Particle size distributions could not be obtained in any case due to intrinsic difficulties associated to the combined effects of very small metal loadings, the nanocrystalline nature of the support which results in a huge number of crystal overlaps and the heavy atomic number of Ce.

IR spectra of CO adsorption performed on the as prepared 0.1Pd–0.36AuCe sample after stopping the reaction at 15 min reaction time (Fig. 6A) shows the presence of an IR band at 2127 cm^{-1} which should be related to $\text{Pd}^{\delta+}$ or $\text{Au}^{\delta+}$ (oxo) species [44], and an IR band at 2098 cm^{-1} ascribed to unsaturated surface sites, probably associated to the small Au particles detected by HRTEM [44]. While

the 2098 cm^{-1} IR band could also be related to unsaturated sites associated to $\text{Pd}(100)$ surface [45–48], HRTEM disregard this possibility since larger Pd crystallites (with a higher saturation degree) could be assumed from the HRTEM data.

A different picture is clearly observed in the reduced 0.1Pd–0.36AuCe sample (active sample) after stopping the reaction at 15 min reaction time. In this case, X-EDS spectra analysis of high intensity areas observed in HAADF-STEM images of this catalyst, using a tiny (0.5 nm) electron probe, show the presence of both Au and Pd signals (atomic composition around 88.68%Au, 11.32%Pd, Pd/Au ratio of 0.13), suggesting the coexistence of both metals in the same particle as it can be seen in Fig. 7. However confirmation

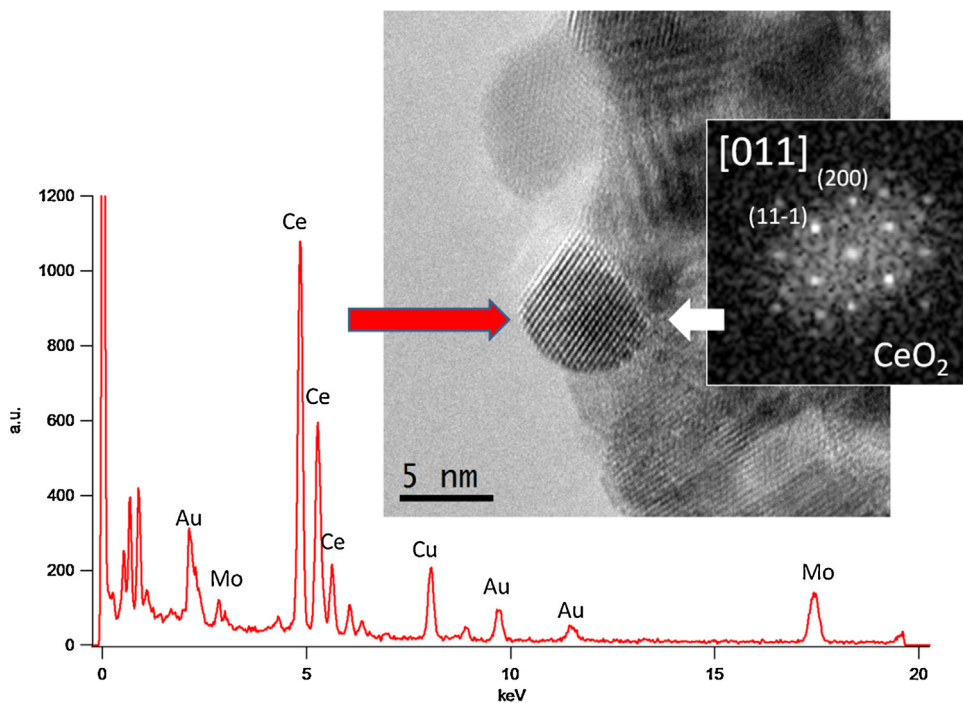


Fig. 5. HTREM image of the as prepared 0.1Pd–0.36AuCe sample after 15 min reaction time. The DDP inset confirms the cubic fluorite-like phase for CeO_2 .

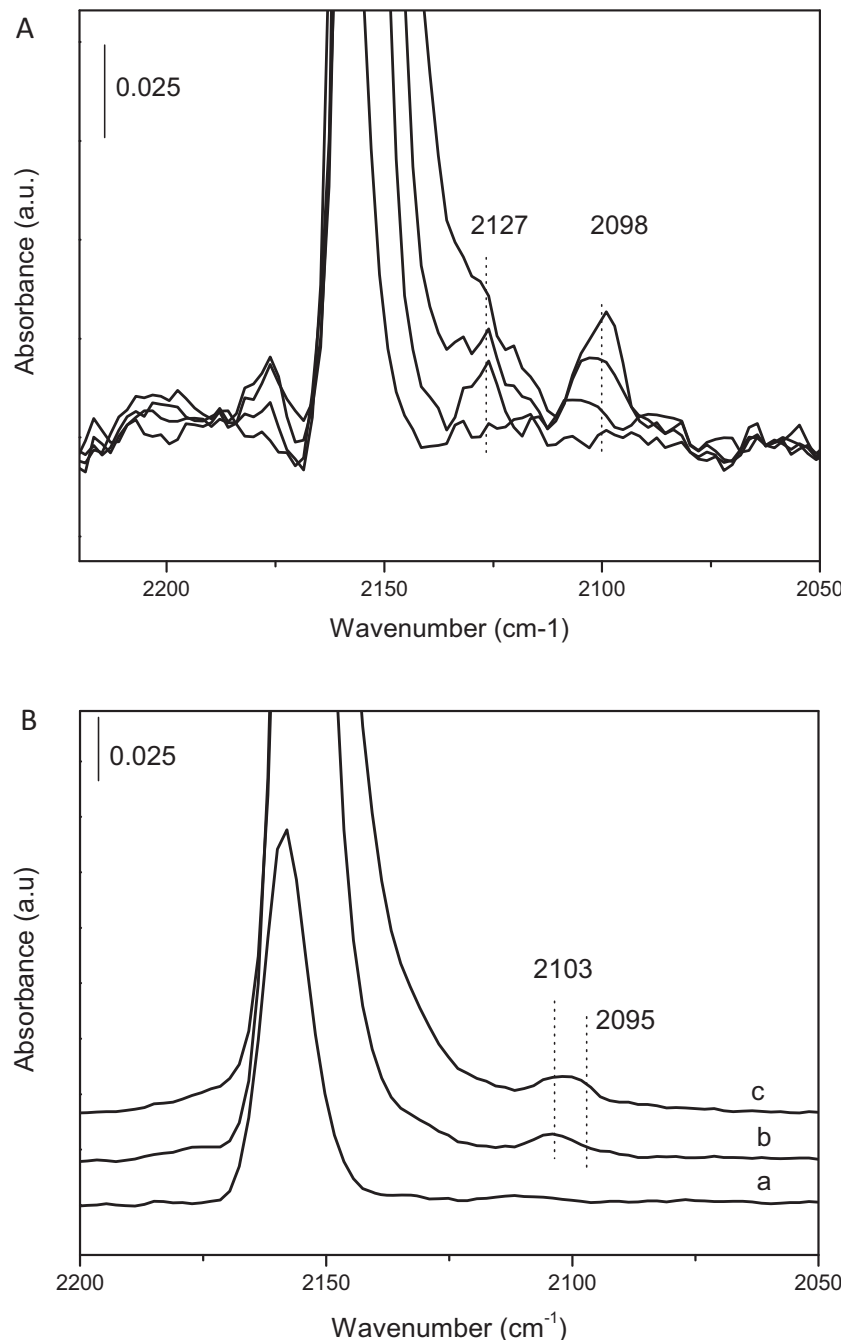


Fig. 6. (A) FTIR spectra of CO adsorption at -176°C at increasing CO coverages (0.2–1 mbar) on as prepared 0.1Pd–0.36AuCe sample after 15 min reaction time. Large saturated IR band at 2155 cm^{-1} assigned either to Au^+ , Ce^{4+} , OH groups [51] or to Pd^{2+} ions [47]. (B) FTIR spectra of CO adsorption at -176°C and 0.2 mbar (a), 0.5 mbar (b) and 1 mbar (c) on ex situ reduced 0.1Pd–0.36AuCe sample, after 15 min reaction time. Large saturated IR band at 2155 cm^{-1} assigned either to Au^+ , Ce^{4+} , OH groups [51] or to Pd^{2+} ions [47]

of a PdAu alloy phase by HRTEM was not possible due to the overlap of the image of these small particles with the contrasts coming from a large number of underlying ceria crystallites. DDPs from the HREM images could only be indexed as corresponding to cubic fluorite CeO_2 . Smaller particles containing only Pd have also been detected, as it is illustrated by the HAADF-STEM and XEDS-STEM studies summarized in Fig. 8.

The surface structure of the reduced 0.1Pd–0.36AuCe sample after stopping the reaction at 15 min reaction time has also been studied by IR spectroscopy of adsorbed CO (Fig. 6B). IR bands in the 2106 – 2098 cm^{-1} region, ascribed to Pd^0 and Au^0 low coordinated metal surface sites are observed, while no IR bands due to large

crystals (at $\sim 2110\text{ cm}^{-1}$) are detected. This agrees with HRTEM data where no large Pd crystallites were detected on the reduced samples after catalytic test.

At this point we can say that HRTEM and FTIR-CO results suggest the coexistence of both Au and Pd metals in the same particle, with an Pd/Au atomic composition of 0.13, together with the absence of big crystallites and the stabilization of small Pd particles, after catalytic test in the most active ex situ reduced 0.1Pd–0.36AuCe sample, while they were not observed in the non-active sample. Moreover a strong restructuration of the surface metal species has been observed after reaction conditions, with gold segregation toward the surface, disrupting the Pd crystal surface. In fact,

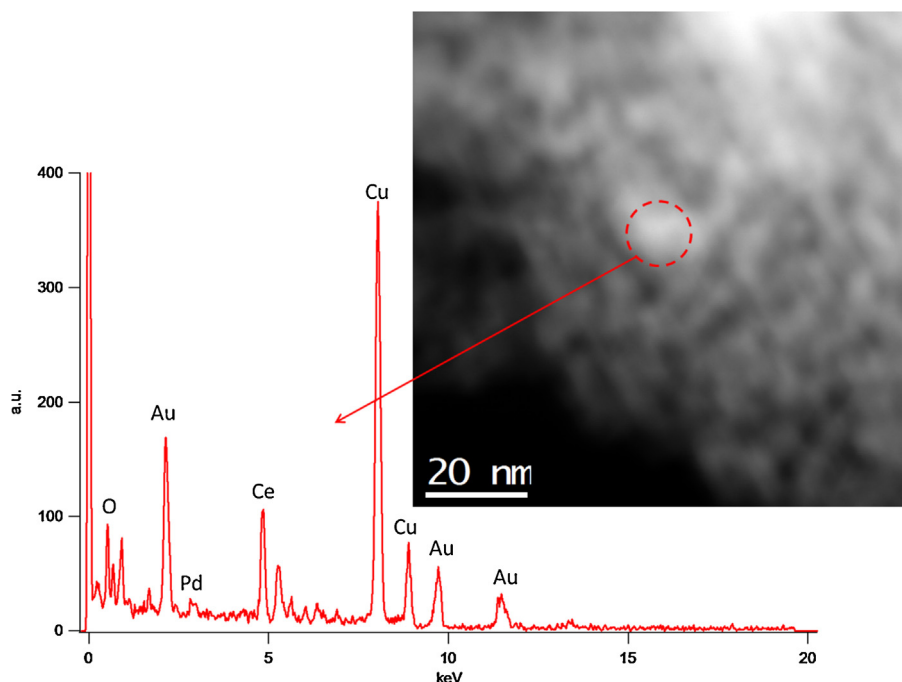


Fig. 7. HAADF-STEM image and XEDS spectra of the reduced 0.1Pd–0.36AuCe sample after 15 min reaction time.

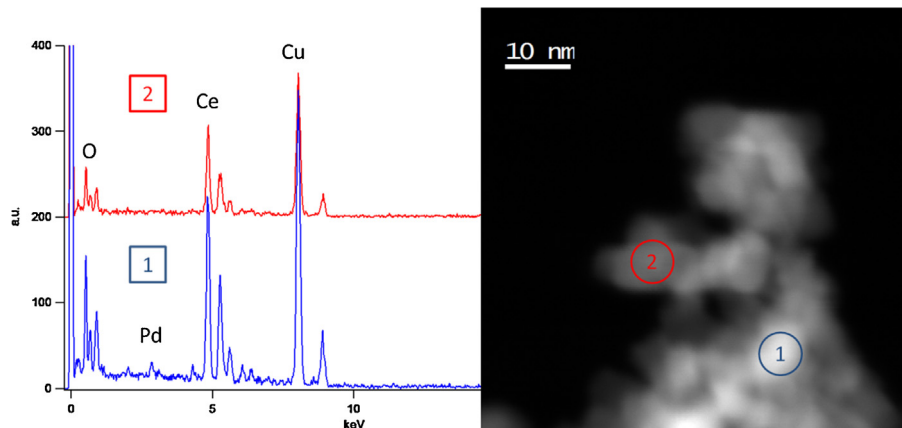


Fig. 8. HAADF-STEM image and XEDS spectra recorded on different spots of the reduced 0.1Pd–0.36AuCe sample after 15 min reaction time. XEDS spectrum from the region marked as 1 on the image peaks both Ce and Pd signals whereas only Ce peaks are observed in the spectrum obtained from 2.

XPS data of the ex situ reduced 0.1Pd–0.36AuCe sample shows a decrease in the Pd/Au molar ratio from 7.4 prior to reaction to 2.6 after reaction, pointing to a decrease of Pd on the surface. This agrees with the FTIR studies of CO adsorption where well faceted Pd crystals observed on the ex situ reduced 0.1Pd–0.36AuCe sample before reaction (Fig. S6, supplementary information) are not more detected once the sample has been exposed to reaction conditions. On the other hand, since the catalytic activity shows a volcano type correlation with the Pd/Au molar ratio, the surface composition of the Au-Pd surface phase should play an important role for catalytic activity. In our case, X-EDS STEM analysis shows a Pd/Au molar ratio of 0.13 for the most active sample. This result implicates isolated Pd surface sites. Moreover the observed drop in the selectivity to isomerization product agrees with the presence of isolated Pd surface sites on the most active sample. However, in detrimental, the selectivity to further hydrogenated product (cyclooctane) increases. This may be related to the

different interaction strength of intermediate products on isolated Pd surface sites [49]. According to Goodman and co-workers [50], the promotional role of Au is to generate isolated Pd monomer sites. Thus these authors attributed the enhanced catalytic activity of Au-Pd catalysts for the acetoxylation of ethylene to vinyl acetate to pairs of Pd monomers.

4. Conclusions

Strong restructuration of AuPd/CeO₂ catalysts is observed after reaction conditions, with gold surface segregation favoring dilution of Pd atoms by Au at the surface of the crystallites. In this sense, the promotional role of Au in our catalysts appears to be related to generate isolated Pd sites, which act as catalytic active sites for the selective hydrogenation of 1,5-COD. This conclusion opens new perspectives for the design of more active and selective catalyst, this being the subject of further investigations.

Acknowledgements

The authors thank the project CSD2009-00050 for financial support. SGG thank the Spanish Ministry of Science and Innovation for financial support through project MAT2011-28009. JCHG and JJCG acknowledge financial support from MINECO/FEDER (Projects MAT2013-40823-R and CSD2009-00013). JCHG acknowledges support from the Ramón y Cajal Fellowships Program of MINECO (RYC-2012-10004).

Appendix A. Supplementary data

Supplementary data associated with this article can be found, in the online version, at <http://dx.doi.org/10.1016/j.cattod.2015.07.022>

References

- [1] S. Alayoglu, F. Tao, V. Altoe, C. Specht, Z. Zhu, F. Aksoy, D.R. Butcher, R.J. Renzas, Z. Liu, G.A. Somorjai, *Catal. Lett.* 141 (2011) 633–640.
- [2] F. Tao, M.E. Grass, Y. Zhang, D.R. Butcher, J.R. Renzas, Z. Liu, J.Y. Chung, B.S. Mun, M. Salmeron, G.A. Somorjai, *Science* 322 (2008) 932–934.
- [3] N.J. Divins, I. Angurell, C. Escudero, V. Pérez-Dieste, J. Llorca, *Science* 346 (2014) 620–623.
- [4] K. Qadir, S.H. Joo, B.S. Mun, D.R. Butcher, J.R. Renzas, F. Aksoy, Z. Liu, G.A. Somorjai, J.Y. Park, *Nano Lett.* 12 (2012) 5761–5768.
- [5] W.C. Chueh, A.H. McDaniel, M.E. Grass, Y. Hao, N. Jabeen, Z. Liu, S.M. Haile, K.F. McCarty, H. Bluhm, F. El Gabaly, *Chem. Mater.* 24 (2012) 1876–1882.
- [6] A. Pulido, P. Concepción, M. Boronat, A. Corma, *J. Catal.* 292 (2012) 138–147.
- [7] Q. Hua, T. Cao, X.K. Gu, J. Lu, Z. Jiang, X. Pan, L. Luo, W.X. Li, W. Huang, *Angew. Chem. Int. Ed.* 53 (2014) 4856–4861.
- [8] T. Ishida, N. Kinoshita, H. Okatsu, T. Akita, T. Takei, M. Haruta, *Angew. Chem. Int. Ed.* 47 (2008) 9265–9268.
- [9] S. Arrii, F. Morfin, A.J. Renouprez, J.L. Rousset, *J. Am. Chem. Soc.* 126 (2004) 1199–1205.
- [10] G.W. Huber, J.W. Shabaker, J.A. Dumesic, *Science* 300 (2003) 2075–2077.
- [11] D.I. Enache, J.K. Edwards, P. Landon, B. Solsona-Espriu, A.F. Carley, A.A. Herzing, M. Watanabe, C.J. Kiely, D.W. Knight, G.J. Hutchings, *Science* 311 (2006) 362–365.
- [12] S. Nishimura, Y. Yakita, M. Katayama, K. Higashimine, K. Ebitani, *Catal. Sci. Technol.* 3 (2013) 351–359.
- [13] L. Kesavan, R. Tiruvalam, M.I. bin Saiman, D.I. Enache, R.L. Jenkins, N. Dimitratos, J.A. Lopez-Sánchez, S.H. Taylor, D.W. Knight, C.J. Kiely, G.J. Hutchings, *Science* 331 (2011) 195–199.
- [14] A. Huidobro, A. Sepúlveda-Escribano, F. Rodríguez-Reinoso, *J. Catal.* 212 (2002) 94–103.
- [15] Q. Zhang, J. Li, X. Liu, Q. Zhu, *Appl. Catal. A: Gen.* 197 (2000) 221–228.
- [16] A. Sárkány, A. Horváth, A. Beck, *Appl. Catal. A: Gen.* 229 (2002) 117–125.
- [17] F. Maroun, F. Ozanam, O.M. Magnussen, R.J. Behm, *Science* 293 (2001) 1811–1814.
- [18] J.K. Edwards, B.E. Solsona, P. Landon, A.F. Carley, A. Herzing, C.J. Kiely, G.J. Hutchings, *J. Catal.* 236 (2005) 69–79.
- [19] G.C. Bond, A.F. Rawle, *J. Mol. Catal. A* 109 (1996) 261–271.
- [20] H. Arnold, F. Döbert, J. Gaube, in: G. Ertl, H. Knözinger, J. Weitkamp (Eds.), *Handbook of Heterogeneous Catalysis*, vol. 5, VCH, Weinheim, 1997, pp. 2165–2186.
- [21] J.P. Boitiaux, J. Cosyns, E. Robert, *Appl. Catal.* 35 (1987) 193–209;
- [22] J.P. Boitiaux, J. Cosyns, S. Vasudevan, *Appl. Catal.* 6 (1983) 41–51.
- [23] A. Sárkány, O. Geszti, G. Sáfrán, *Appl. Catal. A* 350 (2008) 157–163.
- [24] L. Piccolo, A. Piednoir, J.C. Bertolini, *Surf. Sci. Sci.* 592 (2005) 169–181.
- [25] A.K. Krauth, G.H. Bernstein, E.E. Wolf, *Catal. Lett.* 45 (1997) 177–186.
- [26] A.A. Herzing, A.F. Carley, J.K. Edwards, G.J. Hutchings, C.J. Kiely, *Chem. Mater.* 20 (2008) 1492–1501.
- [27] Z. Suo, C. Ma, M. Jin, T. He, L. An, *Catal. Commun.* 9 (2008) 2187–2190.
- [28] H. Liu, G. Mao, S. Meng, *J. Mol. Catal.* 74 (1992) 275–284.
- [29] K. Okitsu, M. Murakami, S. Tanabe, H. Matsumoto, *Chem. Lett.* 11 (2000) 1336–1337.
- [30] Q. Chen, L. Luo, X. Yang, *Indian J. Chem.* 47A (2008) 1317–1322.
- [31] M.P. Kapoor, Y. Ichihashi, T. Nakamori, Y. Matsumura, *J. Mol. Catal. A: Chem.* 213 (2004) 251–255.
- [32] D. Mei, M. Neurock, C.M. Smith, *J. Catal.* 268 (2009) 181–195.
- [33] H. Miura, M. Terasaka, K. Oki, T. Matsuda, *Stud. Surf. Sci. Catal.* 75 (1993) 2379–2382.
- [34] M. Alhumaimess, Z.J. Lin, W.H. Weng, N. Dimitratos, N.F. Dummer, S.H. Taylor, J.K. Bartley, C.J. Kiely, G.J. Hutchings, *Chem. Sus. Chem.* 5 (2012) 125–131.
- [35] J.Y. Chane-Ching, EP 208580, 1987.
- [36] J.K. Edwards, J. Pritchard, L. Lu, M. Piccinini, G. Shaw, A.F. Carley, D.J. Morgan, C.J. Kiely, G.J. Hutchings, *Angew. Chem. Int. Ed.* 53 (2014) 2381–2384.
- [37] R.S. Monteiro, F.B. Noronha, L.C. Dieguez, M. Schmal, *Appl. Catal. A: Gen.* 131 (1995) 89–106.
- [38] K.R. Priolkar, P. Bera, P.R. Sarode, M.S. Hegde, S. Emura, R. Kumashiro, N.P. Lalla, *Chem. Mater.* 14 (2002) 2120–2128.
- [39] J. Batista, A. Pintar, D. Mandrinio, M. Jenko, V. Martin, *Appl. Catal. A: Gen.* 206 (2001) 113–124.
- [40] J. Guzman, S. Carretin, A. Corma, *J. Am. Chem. Soc.* 127 (2005) 3286–3287.
- [41] A. Jablonski, S.H. Overbury, G.A. Somorjai, *Surf. Sci.* 65 (1977) 578–592.
- [42] S. Bernal, J.J. Calvino, M.A. Caquí, J.A. Pérez Omil, J.M. Pintado, J.M. Rodríguez-Izquierdo, *Appl. Catal. B: Environ.* 16 (1998) 127–138.
- [43] M. Boronat, P. Concepción, A. Corma, *J. Phys. Chem. C* 113 (2009) 16772–16784.
- [44] Y. Perez, M.L. Ruiz-González, J.M. González-Calbet, P. Concepción, M. Boronat, A. Corma, *Catal. Today* 180 (2012) 59–67.
- [45] H. Borchert, B. Jürgens, V. Zielasek, G. Rupprechter, S. Giorgio, C.R. Henry, M. Bäumer, *J. Catal.* 247 (2007) 145–154.
- [46] D. Tessier, A. Rakai, F. Bozon-Verduraz, *J. Chem. Soc. Faraday Trans.* 88 (1992) 741–749.
- [47] S. Bertarione, D. Scarano, A. Zecchina, V. Johánek, J. Hoffmann, S. Schauermann, M.M. Frank, J. Libuda, G. Rupprechter, H. Freud, *J. Phys. Chem. B* 108 (2004) 3603–3613.
- [48] D. Childers, A. Saha, N. Schweitzer, R.M. Rioux, J.T. Miller, R.J. Meyer, *ACS Catal.* 3 (2013) 2487–2496.
- [49] M. Chen, D. Kumar, C.-W. Yi, D.W. Goodman, *Science* 310 (2005) 291–293.
- [50] P. Concepción, S. Carretín, A. Corma, *Appl. Catal. A: Gen.* 307 (2006) 42–45.
- [51] P. Concepción, S. Carretín, A. Corma, *Appl. Catal. A: Gen.* 307 (2006) 42–45.